

# Quantifying wetland accretion rates in the Mississippi River Delta using recent crevasse splay deposits as natural analogs for river diversions

Louisiana Sea Grant Undergraduate Research Opportunities Program Report

*Austin Nijhuis*<sup>1</sup>

<sup>1</sup>Department of Earth and Environmental Sciences, Tulane University, 6823 St. Charles Avenue, New Orleans, Louisiana 70118-5698, USA

---

## Abstract

Louisiana has lost approximately one third of its wetlands in the past three centuries. Estimates suggest that an additional ~400,000 acres could be lost by 2050 at the current rate. Land loss has been due to many reasons, including anthropogenic alterations of the river, relative sea-level (RSL) rise, coastal wave erosion, channel construction, etc. The threat of climate change adds to the problem, with the prediction of increased hurricanes and accelerated sea-level rise. River diversion plans for coastal restoration in the Mississippi Delta have been suggested for decades, but implementation has been slow. By studying natural analogs of river diversions such as crevasse splays, it may be possible to improve the understanding about the viability of diverting freshwater and sediment from the Mississippi River into the adjacent wetlands.

This study investigated sediment accretion rates of the Attakapas Splay near Napoleonville, Louisiana, using optically stimulated luminescence (OSL) dating. Lithologic investigation shows that the thickness of the crevasse-splay deposit ranges from 3 to 9 m. Twelve samples from four cores were dated using a single aliquot regenerative dose (SAR) protocol. OSL was measured for 4-11  $\mu\text{m}$  and 75-180  $\mu\text{m}$  quartz grains. OSL dating results demonstrate that the Attakapas Splay was probably formed by multiple crevassing events from 700 to 1200 years ago. Sediment accretion rates were found to be  $>2.5 \text{ cm yr}^{-1}$  for individual crevassing episodes and  $>1 \text{ cm yr}^{-1}$  on average for the entire lifespan of the splay in proximal settings. The

Attakapas Splay was formed by Bayou Lafourche, which likely discharged half of the Mississippi River at the time. Thus, the Bayou Lafourche sediment load may be comparable to that of the present day Mississippi River, which has experienced a reduction of its sediment load by ~50% due to anthropogenic intervention. This study shows that artificial crevassing has significant potential for vertical land growth and long-term wetland stability. Comparing our accretion rates to estimates of present-day rates of eustatic sea-level rise of  $\sim 0.3 \text{ cm yr}^{-1}$  globally and relative sea-level rise (RSL) as high as  $\sim 1 \text{ cm yr}^{-1}$  or more along portions of the Louisiana coast, we conclude that river diversions comparable to crevasse splays are capable of keeping pace with RSL rise and can potentially create new land.

## 1. Introduction

The Mississippi River is the largest river system in North America and its delta is an area of great economic and environmental importance. While the Mississippi River Delta (MRD) provides many benefits to economic and human wellbeing, subsidence, sea-level rise and anthropogenic changes have led to a significant decrease in land area. The delta has lost approximately one-third of its original wetland area in the last hundred years because of human settlement (Gagliano et al., 1981). Estimates suggest that an additional  $\sim 400,000$  acres could be lost by 2050 at the current rate (Coast 2050: Toward a Sustainable Coastal Louisiana, 1998). Wetland loss occurs for many reasons, including anthropogenic alterations of the river, relative sea-level rise, wave erosion, and channel construction.

Without human intervention, the Mississippi River naturally changed its course through time, creating new delta lobes, leaving abandoned lobes to disappear. Wetland loss is accelerated due to human alterations. Humans have altered the movement of freshwater, sediment supply,

and saltwater through levees along the banks and dams upriver (Blum & Roberts, 2009). Dams lead to a reduction in sediment supply, while levees cut off wetlands from the river. Instead of being deposited on the deltaic plain, Mississippi River sediment is channeled through the Mississippi River and carried out to the Gulf of Mexico. Without the replenishment of sediment and nutrients, the deltaic plain is unable to compensate for subsidence and sea-level rise, and the delta eventually drowns (Day et al., 2007, Paola et al., 2010). Restoration of the MRD involves rejoining the channel to the wetlands (Coleman et al., 1998). By reconnecting the river to drowned areas, sediment deposition can build new land and form a foundation for restoring wetlands (Day et al, 2007).

The long-term sustainability of the MRD will have many implications for commercial fishing, recreation, the oil and gas industry, infrastructure, storm-surge protection, human wellbeing, and the ecosystem in general. The benefits of coastal restoration have the potential to be immense in both a local and national scale, especially if hurricane and storm-surge protection is factored in; however, such detail of quantifying economic and environmental benefits will not be done in this paper. Such analysis can be found in Richardson and Scott (2004). Sustainability and adaptation begins with reconnecting the Mississippi River to the wetlands to improve the health of the ecosystem and create vertical land accretion to combat relative sea-level rise. Understanding coastal land growth and being able to model restoration will have significant impacts on how well the MRD and other delta systems of the world can adapt to climate change and relative sea-level rise.

Delta lobes in the MRD were partly created by a series of crevassing events of the river and its major and minor distributaries, such as Bayou Lafourche that lead to floodplain sediment deposits (Aslan and Autin, 1999). Artificial crevasses have been utilized since the 1980s in

managing Louisiana coastal environments (Troutman and MacInnes, 1999). An improved understanding of these artificial and natural crevasse splays can serve as a valuable tool for future restoration projects. By determining past sediment accretion rates, it can be seen if a river diversion is able to offset relative sea-level rise in the present. While there are varying exogenous factors, such as sediment supply, natural crevasse splays can be used as a natural analog to gain a better understanding of the potential impact of river diversions in coastal restoration.

In this study, the Attakapas Splay (Fig. 1) was examined to investigate wetland accretion rates of a crevasse splay. A LIDAR map shows that this was crevassing event of Bayou Lafourche when it was a major channel of the Mississippi River (Törnqvist et al., 1996). The sediment supply of Bayou Lafourche during this crevassing event may be analogous to present day Mississippi River supply, which has lost ~50% of its sediment supply due to human intervention. Samples were taken by hand drilling for optically stimulated luminescence (OSL) dating purpose to determine the sediment accretion rate of the Attakapas Splay. A total of 12 samples were taken from four cores (Fig. 1). Quartz grains of the 75-180  $\mu\text{m}$  or 4-11  $\mu\text{m}$  range were extracted for OSL dating purposes. OSL dating was performed using the single aliquot regenerative dose (SAR) protocol outlined in Murray & Wintle (2000, 2003) to measure the equivalent dose. From this, estimates of age and accretion rates were made. The results suggest that a crevasse splay can be used as analog to river diversions and a model to adapt to RSL rise and potentially create significant vertical land.

## **2. Study Area**

Fieldwork took place near Napoleonville, Louisiana, USA from April 2010 to early June 2010. Hand-drilling cores were used to construct subsurface cross-sections, determine lithology according to the United States Department of Agriculture (USDA) soil classification system, to provide information for OSL sample location selection, and to obtain samples for OSL dating purposes.

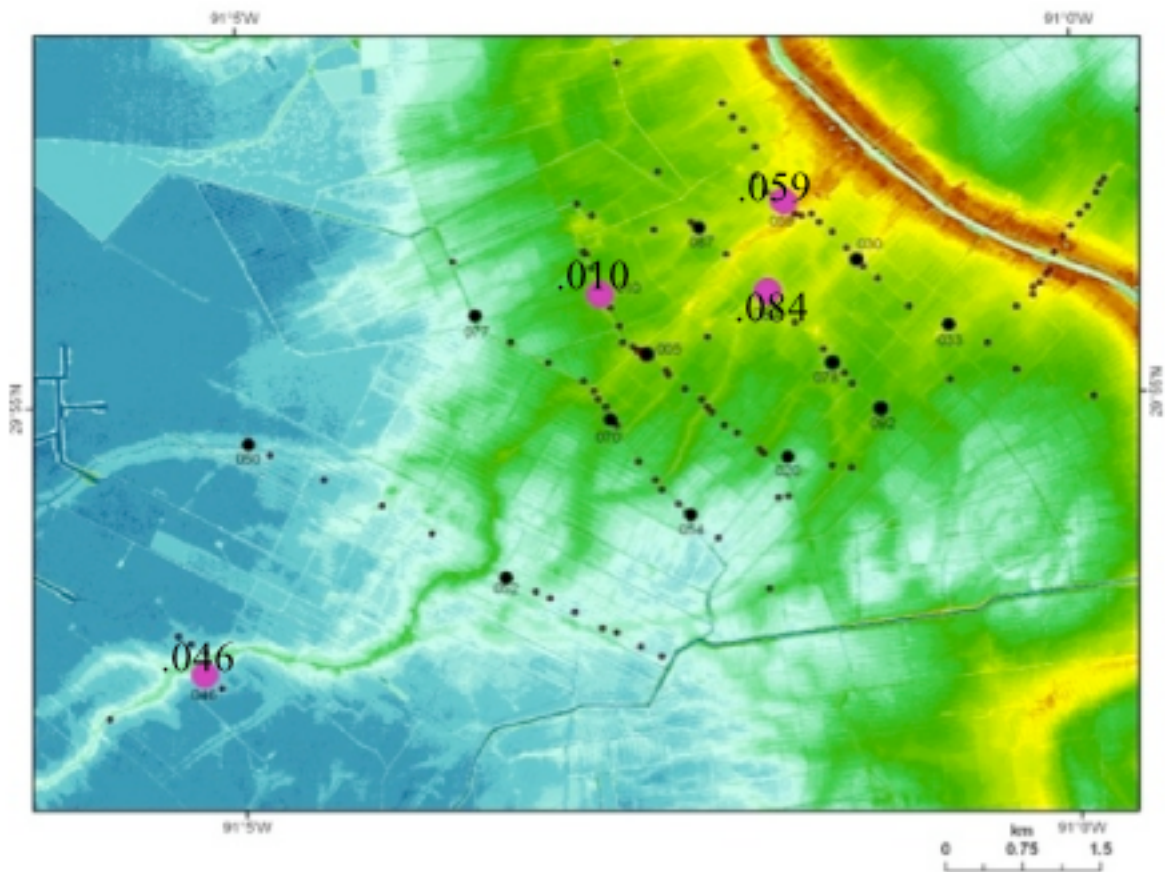


**Figure 1. LIDAR map of Attakapas Splay field site with core sites for lithologic investigation (small indicators) and for OSL dating (large indicators). Cores 1094.046, .010, .084, .059 were dated in this paper.**

### 3. Background

### 3.1 Background of optically stimulated luminescence dating

#### 3.1.1 The energy band model

To understand optically stimulated luminescence (OSL), it is particularly helpful to begin with an introduction of the energy band model (Fig. 2). The energy band model describes the behavior of electrons of a mineral crystal to external forces, such as ionizing radiation, heat and light. In a perfect crystal, there are two allowed energy states, one is in the conduction band and the other is in the valence band. The conduction band is the higher energy band of the allowed states and is usually empty of electrons. The valence band is the lower energy band of the allowed states. Electrons are stored in the valence band because they have the tendency to fill the lowest energy states. The gap between the two bands is called the band gap the energy needed for an electron to “jump” from the valence band to the conduction band is called the band gap energy. The equation for band gap energy is as given as follows:

$$E_g = E_c - E_v \quad (\text{Eq. 1})$$

where  $E_g$  is the band gap,  $E_c$  is the lowest energy state in the conduction band and  $E_v$  is the highest energy state in the valence band.

As an external force is applied, such as through ionizing radiation, electrons in the valence band absorb energy and are evicted to the conduction band when they have enough energy to overcome the band gap ( $E_{\text{external}} \geq E_g$ ). When an electron reaches the conduction band, it leaves a hole in the valence band. Once an electron gets to the conduction band, it resides there for a fraction of a second until it drops back down to the valence band and loses energy in the forms of heat, light, or by transferring the energy to another electron.

A crystal structure, however, is not perfect and contains different defects. Crystal defects create localized charge deficits that can temporarily capture electrons. These defects create allowed energy states in the band gap. If a crystal defect can capture an electron (or holes) from the conduction band (or valance band), the defect is called an electron trap (or a recombination center). Electron can remain trapped until external forces (heat, light) evict the electron to the conduction band. While the electrons recombine with trapped holes through radiative recombination, thermoluminescence (TL) is emitted when the external force is heat and optically stimulated luminescence (OSL) when it is light.

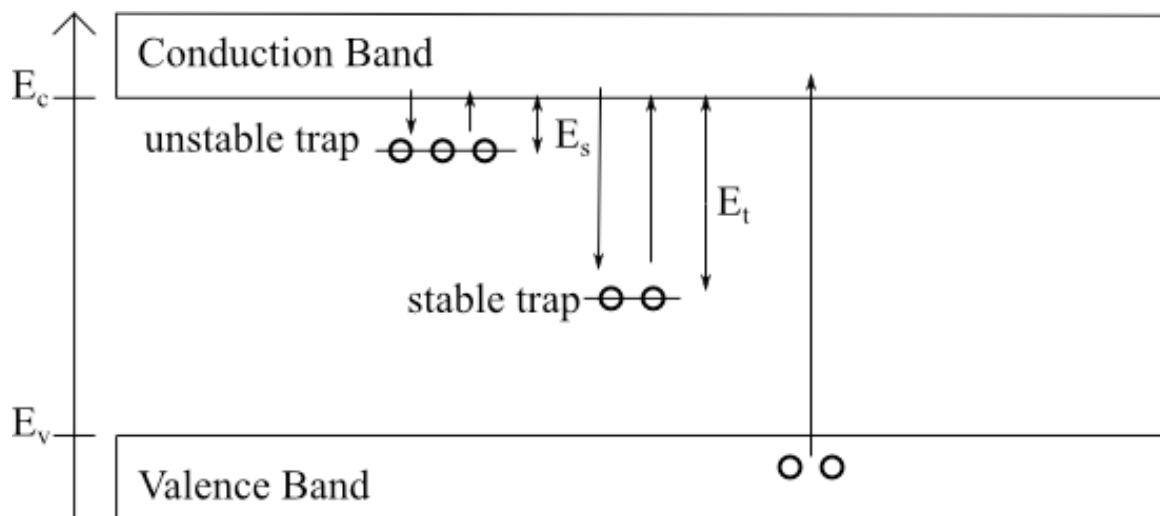


**Figure 2. Energy band model.** Figure adapted from (Thomsen, 2004). This figure shows the energy band model. As a force is applied, electrons jump from the valence band to the conduction band. In the presence of crystal defects, electrons may be charged in stable or unstable traps. The energy needed for eviction from these traps is represented as  $E_s$  for unstable traps and  $E_t$  for stable traps.

### 3.1.2 Optically stimulated luminescence dating

The natural accumulation of trapped electrons is mainly a result of exposure to nuclear radiation from potassium-40, thorium, and uranium, with minor contributions from rubidium and cosmic rays (Aitkin, 1998). Trace amounts of these elements and cosmic rays are naturally occurring in sediment. Nuclear radiation is emitted when the nuclei of these elements undergo radioactive decay. The ionizing radiation produced by these radioactive elements can be absorbed in minerals, such as quartz and feldspar, as well as in water and organic matter. The resulting nuclear damage to the quartz or feldspar crystal structure creates charged electron traps that trap electrons as the electrons jump across the band gap when an external force is applied.

At low energy doses the number of trapped electrons is proportional to the absorbed dose (measure of energy deposited in a medium by ionizing radiation) in the material. When the trapped charge is released and the light emitted in the process is measured, assessment of the absorbed dose is possible. The absorbed dose can be calculated by comparing the natural OSL signal to OSL signals induced in the laboratory from known doses. The laboratory dose that would induce OSL signal identical to the natural OSL signal is called the equivalent dose,  $D_e$ . With  $D_e$  and the dose rate (the rate at which energy is absorbed), the age of the last deposition event of the sediment sample can be estimated with the equation:

$$\text{Age (ka)} = \text{Equivalent dose (D}_e\text{) (Gy)} / \text{dose-rate (Gy ka}^{-1}\text{)} \quad (\text{Eq. 2})$$

### *3.1.3 Applications*

The basic concepts of luminescence dating are shown in Figure 3. When the electron traps are completely emptied, either through exposure to light or heat, the OSL signal is “zeroed.” This event, often called a “bleaching event,” represents the last time the sediment was

exposed to light, such as during deposition prior to burial in fluvial sediment. After the zeroing event, the OSL signal starts to rebuild because of natural nuclear radiation. In the lab, a known radiation dose is applied to the quartz or feldspar grains to estimate the  $D_e$ . The dose-rate is determined from the concentrations of uranium, thorium and potassium. With the equivalent dose and dose rate, it is possible to estimate the time of the last bleaching event.

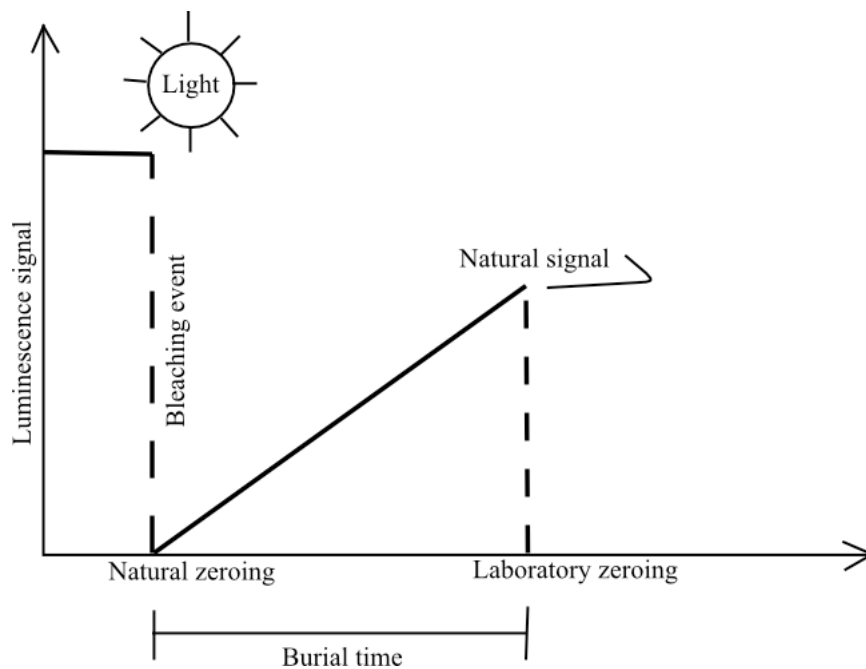


**Figure 3. Basic concepts of luminescence.** Figure adapted from (Aitkin, 1998). The last time sediments were exposed to light, such as in a depositional event, it is optically zeroed. Over time, the luminescence signal grows in quartz and feldspar by absorbing radiative energy. The luminescence signal is measured in the lab to determine the equivalent dose.

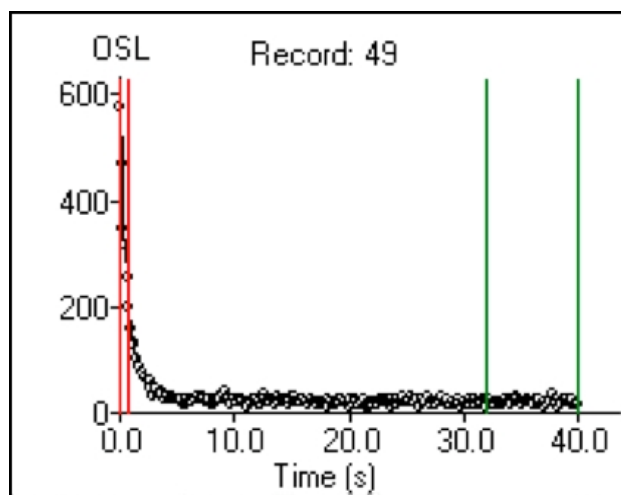


**Figure 4. OSL decay-curve.** The fast component component was bleached in the first few seconds. Slower components take longer to be completely bleached. Slow components make up a portion of the background in the last section of the decay curve.

OSL measurements, in this study, were performed using the *Continuous wave-OSL mode* (CW-OSL). With this mode, a sample is stimulated with a constant light intensity for a given time, while the luminescence emission is monitored during stimulation. The luminescence emission is measured at a different wavelength than the stimulation wavelength. As stimulation time increases, the luminescence signal decreases because electron traps are being depleted. This processes of the OSL signal declining until a signal reaches a constant background level is shown in an OSL decay curve (Fig. 4). OSL can be described as a combination of fast, medium, and slow components (Bailey et al., 1997). The traps that contribute to the fast component are very sensitive to optical stimulation. These traps are depleted almost instantly by light (natural or artificial). Traps that are weakly sensitive to optical stimulation make up the slow component and would require longer stimulation times to be emptied. OSL dating focuses on the traps that are most light sensitive and most likely to have been well zeroed at burial. To extract the fast and

medium components, the background is subtracted from the initial OSL signal of the decay curve. The net signal is used in OSL analysis (Wintle & Murray, 2006).

### 3.2 Equivalent dose estimation

The natural OSL signal is measured in the laboratory as light-sensitive electron traps are emptied. A known laboratory dose,  $D_i$ , is then given to the sample to measure a regenerated OSL signal. By repeating regeneration doses with varying doses, a dose response curve can be constructed (Fig. 5). The dose response curve shows how the OSL signal increases as radiation dose increases. The natural OSL signal can be interpolated onto the dose-response curve by plotting the natural OSL signal to find the equivalent dose needed to induce an OSL signal equivalent to the natural OSL signal.

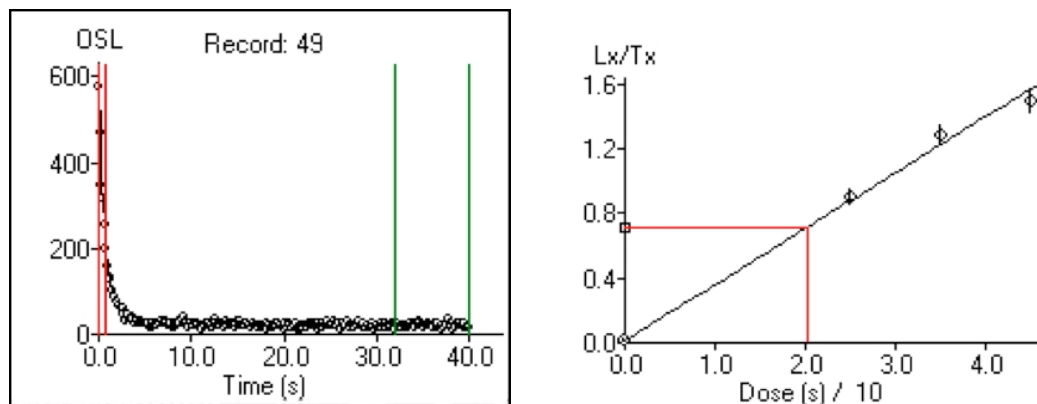


**Figure 5. OSL-decay curve and dose response.** The natural OSL signal is determined in the decay curve. Known laboratory doses are given to the aliquots to produce a dose response curve. By transposing the natural dose onto the growth curve, the  $D_e$  can be determined. This  $D_e$  is an estimation of the paleodose, or dose required to induce signal equivalent to the natural signal.

Laboratory experiments have shown that the OSL signal is generated from stable and unstable traps. To accurately compare natural and regenerated signals, the unstable traps must be

removed. This is commonly done through preheating the sample between 160 °C and 300 °C to remove the unstable signal (Aitkin, 1998). Heating quartz aliquots, however, alters the sensitivity (or emitted luminescence per unit dose) of the sample. The single-aliquot regenerative-dose (SAR) protocol was developed to overcome the problem of sensitivity changes by monitoring and correcting sensitivity changes with the OSL of a test dose (Murray & Roberts, 1998).

## 4. Methods

### 4.1 Sample preparation

Sample preparation was carried out in the dark room facilities at Tulane University with amber (591 nm) light. A total of twelve samples were processed from four cores. The cores, depths, textures, measured grain sizes, and sample names are listed in Table 1. The first step was removing the outer ~1cm layer of the core that was exposed to light during sample collection. The exposed sample was stored for later use for water content and natural radioactivity measurements. Coarse and fine-grained sediments were prepared with two different methods.

**Table 1**  
**Sample names and characteristics**

<b>1094.010</b>			
<b>Depth (cm)</b>	<b>Texture</b>	<b>Grain size (µm)</b>	<b>Sample ID</b>
110-120	SL	75-180	TUOSL 22
410-420	SiL	75-180	TUOSL 23
590-600	SiCL	4-11	TUOSL 24
<b>1094.059</b>			

<b>Depth (cm)</b>	<b>Texture</b>	<b>Grain size (<math>\mu\text{m}</math>)</b>	<b>Sample ID</b>
190-200	vfs-fs	75-180	TUOSL 26
300-310	SL	4-11	TUOSL 27
530-540	SL	75-180	TUOSL 28
720-730	SL	75-180	TUOSL 29

---

**1094.084**


---

<b>Depth</b>	<b>Texture</b>	<b>Grain size (<math>\mu\text{m}</math>)</b>	<b>Sample ID</b>
130-140	SL	75-180	TUOSL 30
410-420	vfs	75-180	TUOSL 31
690-700	SiC	4-11	TUOSL 32

---

**1094.46**


---

<b>Depth</b>	<b>Texture</b>	<b>Grain size (<math>\mu\text{m}</math>)</b>	<b>Sample ID</b>
140-150	SiL	4-11	TUOSL 33
650-660	SiL	4-11	TUOSL 35

---

#### *4.1.1 Coarse-grained samples*

Coarse-grained samples were wet sieved in 75 and 180  $\mu\text{m}$  sieves in order to collect grains within the 75-180  $\mu\text{m}$  range. Samples were then treated with  $\text{H}_2\text{O}_2$  to remove organic matter and HCl to remove carbonate material. 10% concentrations were initially used to prevent overreaction and then the concentration was increased to 35%. The process was complete when no reaction occurred and the samples were neutralized with NaOH after completion. Table 2 shows the amount and number of times of  $\text{H}_2\text{O}_2$  and HCl treatment for each sample. The coarse-grained samples were then treated to separate heavy minerals from quartz and feldspar. The

removal of heavy metals, such as zircon, is important because these minerals give off a high luminescence signal. To remove heavy minerals, the samples underwent heavy liquid separation, with a heavy liquid with a density of 2.75 g/mL. Quartz was separated from feldspar using heavy liquid with a density of 2.62 g/mL.

#### 4.1.2 Fine-grained samples

Fine-grained samples were sieved through a 75  $\mu\text{m}$  sieve and treated with  $\text{H}_2\text{O}_2$  and  $\text{HCl}$  in the same procedure as the coarse-grained samples were (Table 2). 4-15  $\mu\text{m}$  grains were separated using sedimentation cylinder separation using Stoke's Law, an equation relating the terminal velocity of a smooth sphere in a viscous fluid and viscosity to the diameter of the sphere when subjected to a known force (gravity). This process also removes some heavy minerals and mica.

**Table 2**  
**Sample Preparation, Removal of Organics and Carbonates**

	TUOSL 22	TUOSL 23	TUOSL 24	TUOSL 26	TUOSL 27
<b>Removal of Organics</b>	<b># of Times</b>	<b># of Times</b>	<b># of Times</b>	<b># of Times</b>	<b># of Times</b>
25 mL 10% $\text{H}_2\text{O}_2$	3	3	3	3	3
25 mL 35% $\text{H}_2\text{O}_2$	2	2	2	2	1
<b>Removal of Carbonate</b>					
25 mL 10% $\text{HCl}$	2	2	2	2	2
	TUOSL 28	TUOSL 29	TUOSL 30	TUOSL 31	TUOSL 32
<b>Removal of Organics</b>	<b># of Times</b>	<b># of Times</b>	<b># of Times</b>	<b># of Times</b>	<b># of Times</b>
25 mL 10% $\text{H}_2\text{O}_2$	2	2	2	2	2
25 mL 35% $\text{H}_2\text{O}_2$	2	2	2	2	1
<b>Removal of Carbonate</b>					
25 mL 10% $\text{HCl}$	2	2	1	2	2

	TUOSL 33	TUOSL 35
<b>Removal of Organics</b>	<b># of Times</b>	<b># of Times</b>
25 mL 10% H <sub>2</sub> O <sub>2</sub>	2	2
25 mL 35% H <sub>2</sub> O <sub>2</sub>	1	2
<b>Removal of Carbonate</b>		
25 mL 10% HCl	1	1

#### 4.3 Hydrofluoric Acid (HF) etching

Feldspar can contribute to and underestimate the equivalent dose. Thus, hydrofluoric acid (HF) is added to prevent feldspar contamination, using the process outlined in Mauz and Lang, 2004, which showed that high concentrations of HF mixed for a short period of time is best for removing feldspar. 20% and 48% HF was used at varying time intervals as shown in Table 3.

**Table 3**  
**Concentration of HF added and time for each sample**

1094.010			1094.084		
Sample	Conc. [HF] (%)	Time (min)	Sample	Conc. [HF] (%)	Time (min)
TUOSL 22	48	20	TUOSL 30	48	60
TUOSL 23	48	40	TUOSL 31	48	60
			TUOSL 32	20	20
1094.059			1094.46		
Sample	Conc. [HF]	Time (min)	Sample	Conc. [HF]	Time (min)
TUOSL 26	48	20	TU33	20	10
TUOSL 27	20	20	TU35	20	20
TUOSL 28	48	60			
TUOSL 29	20	20			

#### 4.4 Preparing aliquots

Aliquots (subsamples) of each sample were mounted on stainless steel (coarse-grained) and aluminum (fine-grained) discs, 1 cm in diameter. Coarse-grained aliquots were prepared by placing grains on silicone gel placed on the center of the disc, ~1 mm in diameter. Fine-grained aliquots were prepared using acetone evaporation. Equal proportions of sediment were mixed with acetone, which was allowed to evaporate, leaving the sediment on the aluminum discs.

#### 4.5 Water content

Water absorbs radiative energy and contributes to the dose rate. Thus, the outer layer removed from sample cores was measured for water content. This was done by measuring the initial mass of the wet sediment, drying it in an oven at ~100 °C for ~24 hours. The dry mass was then measured. The water content was calculated with Eq. 3 and the results are in Table 4.

$$\text{Water Content (\%)} = \text{Water Mass (g)} / \text{Wet Sediment Mass (g)} * 100\% \quad (\text{Eq.3})$$

**Table 4**  
**Water Content**

Sample	Mass of Container (g)	Container + wet (g)	Container + dry (g)	Water Mass (g)	Water Content (%)
TUOSL 22	10.15	150.79	119.70	31.09	22.11
TUOSL 23	10.10	150.56	116.20	34.36	24.46
TUOSL 26	10.1	150.56	120.57	29.99	21.35
TUOSL 27	10.11	149.46	113.09	36.37	26.10
TUOSL 28	10.16	149.98	115.54	34.44	24.63
TUOSL 29	10.15	149.75	101.19	48.56	34.79

TUOSL 30	10.21	150.39	116.94	33.45	23.86
TUOSL 31	10.07	150.87	115.81	35.06	24.90
TUOSL 32	10.09	150.08	99.50	50.58	36.13
TUOSL 33	10.01	149.43	110.43	39.00	27.97
TUOSL 35	10.39	150.58	108.56	42.02	29.97

#### *4.6 OSL measurements*

OSL measurements were taken at the Optically Stimulated Luminescence Laboratory at the Department of Geography at the University of Liverpool, Liverpool, UK. The laboratory contains a Risø DA-15 automated TL/OSL reader equipped with a  $^{90}\text{Y}/^{90}\text{Sr}$ -source, delivering  $\sim 5.6 \text{ Gy min}^{-1}$ , 41 blue LED's, and a 1W IR laser diode, and a Risø DA 15B/C automated TL/OSL reader equipped with a  $^{90}\text{Y}/^{90}\text{Sr}$ -source, delivering  $\sim 7.3 \text{ Gy min}^{-1}$ , 21 blue LED's, and 21 IR LED's.

##### *4.6.1 Preheat test*

As outlined in the generalized procedure for the SAR protocol, it is standard practice to preheat samples before OSL measurement. In the preheat test, a series of equivalent dose determinations are made using preheat temperatures of increasing strength and equivalent doses of the same sample are plotted against the temperature of preheat. Based on the preheating test, the optimal preheat temperature was found to be  $200 \text{ }^{\circ}\text{C}$ .

##### *4.6.2 Dose Recovery Test*

A dose recovery test is run to test whether a known laboratory dose can be recovered using the SAR protocol (Murray and Wintle, 2003). In this test, a sample is completely optically zeroed and administered a known laboratory dose. The aliquots are measured and the measured dose is compared to the given test dose, using the SAR protocol. This measures the reliability of the protocol by examining the ratio between the known test dose and the measured dose; if the ratio is unity or near unity, the SAR protocol is reliable.

#### *4.6.3 Measuring Equivalent Dose Using SAR*

The equivalent dose was measured using the generalized SAR protocol outlined in Murray and Wintle, (2000, 2003). Aliquots were preheated at 200 °C for 10 s. The natural OSL signal  $L_N$  was measured, subsequently. The aliquots were then given a known test dose  $D_T$  and heated to 160 °C, cooled, and then the OSL signal  $T_N$  from the test dose was measured. This cycle was repeated again by giving the first regenerative dose  $D_1$  to the sample. The regenerated signal  $L_1$  was measured after preheating at 200 °C for 10 s. The sample was then given the same test dose  $D_T$ , heated and the induced signal  $T_1$  measured. The OSL response to  $D_T$  is used to measure sensitivity changes in measurements. By dividing  $L_i/T_i$ , a sensitivity corrected OSL is found. This process of giving a regenerative dose  $D_i$  (with varying  $D_i$ ) and a test dose  $D_T$  was repeated multiple times, with regenerative doses bracketing the expected natural dose. A regenerative dose was also repeated to determine if the correction for sensitivity change works properly. If the sensitivity change works properly, the corrected OSL ratio should remain constant for a fixed  $D_i$  (if  $D_5 = D_1$ , then  $L_5/T_5$  should be identical to  $L_1/T_1$ ). A sensitivity corrected dose response curve is made by plotting values of  $L_i/T_i$  as a function of dose.

The SAR protocol also addresses the possibility of thermal transfer or recuperation. If no dose is given to the sample ( $D_i = 0$  Gy), there should be no OSL signal observed. However, if significant amount of OSL signal is observed, it can be caused by thermal transfer. If the recuperation ratio is  $\sim 0\%$  ( $< 5\%$ ), then no electrons were recuperated during preheating and there was no OSL signal detected when a test dose of 0 Gy was administered. The Post IR OSL/OSL ratio measures feldspar contamination (Duller, 2003). The regenerative dose is repeated a third time. Before the repeated regenerative dose is administered, the sample is shined with infrared LED's, which bleaches feldspar grains. If the aliquot is contaminated with feldspar, then  $L_5/T_5 \neq L_1/T_1$ . Table 5 shows a detailed outline of the OSL measurement sequence. Regenerative doses of  $\sim 1.6$  Gy,  $\sim 2.4$  Gy, and  $\sim 3.2$  Gy were given. The regenerative dose of 1.6 Gy was repeated twice to check for sensitivity changes and feldspar contamination.

**Table 5**  
**Outline of OSL measurement procedure**

Step	Treatment	Observed
1	Sample given dose $D_N$ at burial	-
2	Preheat for 10s at $200^\circ\text{C}$	-
3	Stimulate at $125^\circ\text{C}$	$L_N, L_{20}, \dots, L_i$
4	Give test dose $D_t$	-
5	Heat to $160^\circ\text{C}$	-
6	Stimulate at $125^\circ\text{C}$ to measure signal from $D_t$	$T_N, T_{20}, \dots, T_i$
7	Return to 1 with shine-down time of $20 \text{ s}^{\text{ab}}, 30 \text{ s}, 40 \text{ s}$	-

<sup>a</sup> Repeat 20 s to measure for sensitivity changes

<sup>b</sup> Repeat another time, shining IR LED before stimulation to check for feldspar contamination

The criteria for acceptance were recycling ratios between 0.90 and 1.10 and a recuperation ratio <5%. As can be seen in the data (Fig. 8), there is scatter of equivalent doses between aliquots in a sample. Using single aliquots with few grains makes it possible to single out the aliquots that best represent the age of deposition. Partially bleached samples will lead to higher estimations of the equivalent dose because electrons were not completely bleached at deposition. If aliquots are not uniformly bleached, there will be a degree of scatter seen in the individual estimates of the sample. The degree of scatter is dependent on the amount of grains in each aliquot (Duller, 2008). Reducing the number of grains in each aliquot makes partially bleached aliquots more easily identified. The best estimate of the equivalent dose is found from the grains with the smallest equivalent doses.

For coarse-grained samples, the minimum age model (Galbraith et al., 1999) was used to determine the equivalent doses. The model assumes that some grains have been fully bleached at deposition, while others have been partially bleached. The minimum age model truncates the partially bleached grains and measures the fully bleached grains using statistical analysis. Olley et al., (2004) conclude that the minimum age model is the most appropriate method to determine burial ages of Holocene sediments. For fine-grained samples, mean and standard deviation was used to estimate the equivalent dose, because there is no way to detect partial bleaching of fine grains so far.

## 4.7 Dose rate determination

**Table 6**  
**Concentrations of  $^{238}\text{U}$ ,  $^{232}\text{Th}$ ,  $^{40}\text{K}$ , and dose rate**

Sample	[ $^{238}\text{U}$ ] $\mu\text{g/g}$	[ $^{232}\text{Th}$ ] $\mu\text{g/g}$	[ $^{40}\text{K}$ ] $\mu\text{g/g}$	Dose rate ( $\text{Gy yr}^{-1}$ )
TUOSL 22	2.82	7.93	1.81	0.16
TUOSL 23	3.52	10.68	1.78	0.17
TUOSL 26	2.92	8.99	1.79	0.15
TUOSL 27	3.76	10.86	1.93	0.14
TUOSL 28	3.01	8.24	1.75	0.15
TUOSL 29	4.54	12.65	2.21	0.12
TUOSL 30	5.55	16.82	1.84	0.29
TUOSL 31	3.74	11.15	1.74	0.16
TUOSL 32	4.74	13.72	2.55	0.14
TUOSL 33	3.08	10.30	2.11	0.13
TUOSL 35	3.85	11.22	2.12	0.13

A basic assumption is that the natural dose rate does not change significantly throughout time.  $\gamma$ -spectrometry was used to estimate the natural dose rate, using material from dried samples that were grinded down using a mortar and pestle and placed in a sealed container. Samples were stored for a month and then analyzed with high-resolution  $\gamma$ -spectrometry to obtain the concentrations of  $^{232}\text{Th}$ ,  $^{40}\text{K}$ , and  $^{238}\text{U}$ . The natural dose rate was calculated according to Adamiec and Aitken (1998). The in situ water content was used and a quartz  $\alpha$ -value of 0.03 was applied (Mauz et al., 2006). With the  $D_e$  and the dose rate the age of the samples can be estimated using variations of the age equation (Eq. 2).

## 5. Results and Analysis

### 5.1 Preheat Test

Fig. 6 shows the results for the preheat test of TUOSL 23. Twenty aliquots of TUOSL 23 were used with the SAR protocol. Four aliquots were used at temperatures of 160 °C, 180 °C, 200 °C, 220 °C, and 240 °C, respectively and each aliquot was preheated for 10 s. The recycling ratio and Post-IR OSL/OSL ratio were plotted to check sensitivity correction and feldspar contamination and the recuperation ratio was plotted to check for thermal transfer. There is a stable plateau in equivalent dose from 160 °C to 200 °C, meaning that the optimal preheat temperature is within the range of 160-200 °C. The equivalent dose rises at temperatures above 200 °C. The accuracy of equivalent dose measured at 200 °C (less scatter), and recycling ratios between 0.9 and 1.1, and a recuperation ratio <5%, led to the selection of 200 °C for 10 s for the optimal preheat for samples.

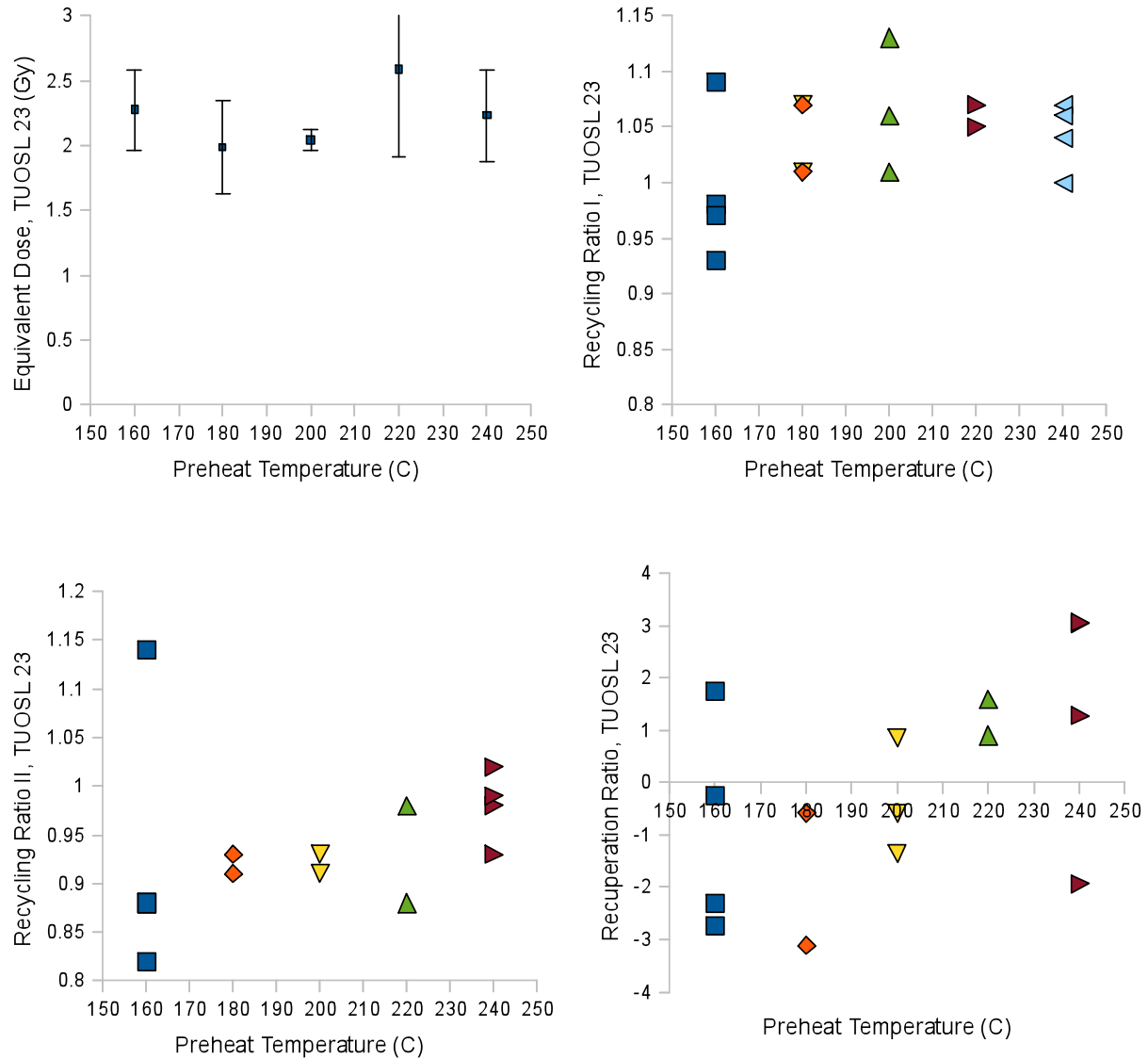


**Figure 6. Plots of equivalent dose, recycling ratio, and recuperation ratio vs. preheat temperature for TUOSL 23.**

### 5.2 Dose Recovery Test

Fig. 7 shows the dose recovery ratios of TUOSL 22, 23, 26, and 29. The dose recovery ratio is near unity, taking into account measurement error, meaning the SAR protocol is reliable.

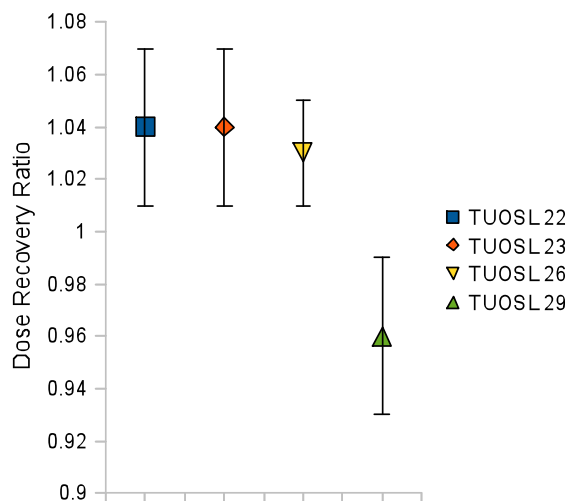


**Figure 7. Dose recovery ratio obtained from measurement of 4 samples.**

### 5.3 Equivalent dose estimation

The lithology and location of the sampled OSL cores are shown in Fig. 9 and labeled *1094.010*, *1094.059*, *1094.085*, and *1094.046*. A histogram of measured equivalent doses for each OSL sample is shown in Fig. 8. The lithology and ages of these cores show the crevasse splay occurring above the peat layer and that the splay was very silty. The ages and lithology suggest that there were two dated depositional events in cores 1094.059 and 1094.084.

Deposition ranged from ~3-9 m of sandy and silty material. The equivalent doses found using the mean and minimum age model are seen in Table 7. With equivalent dose and dose rate, age estimates can be made. The ages are shown in Table 8.

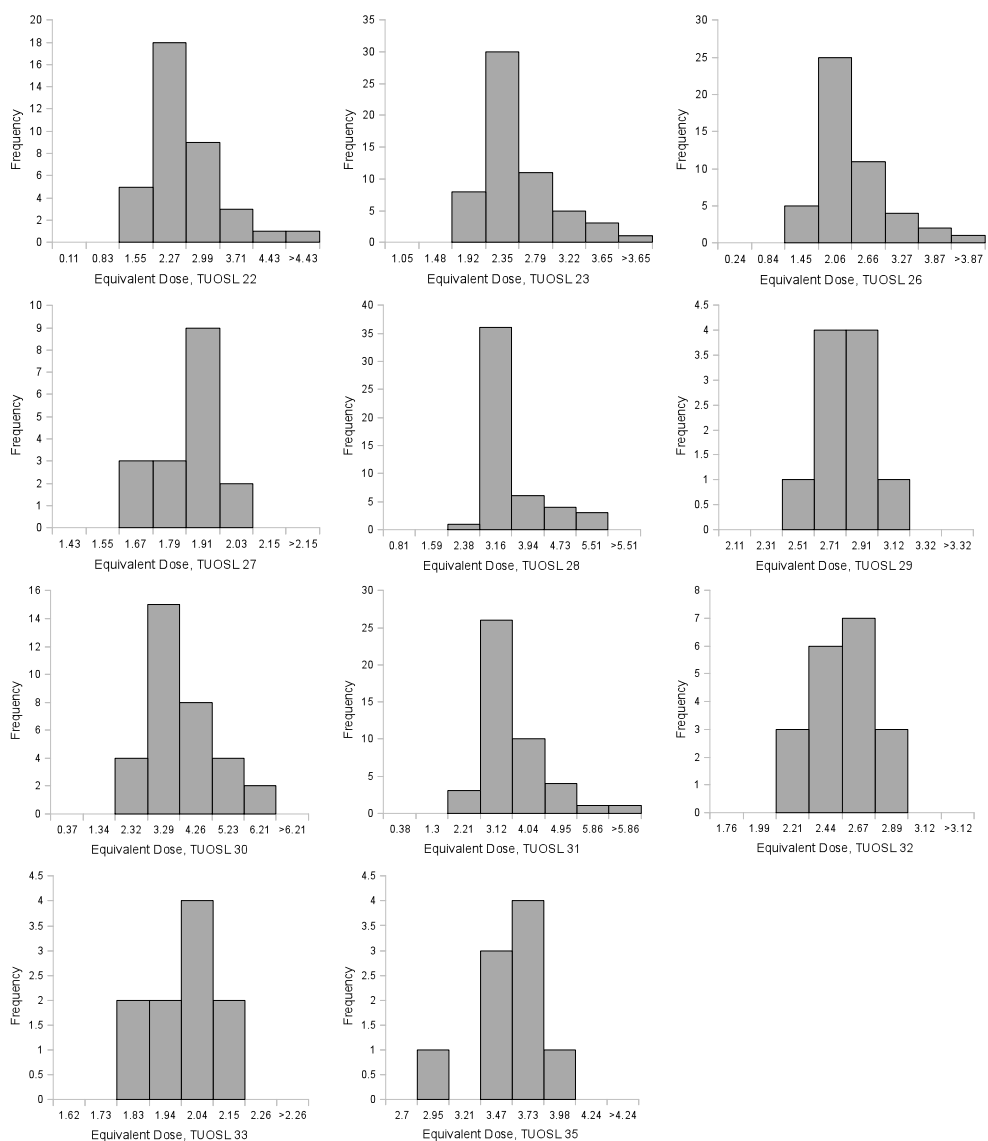


**Figure 8. Histogram of measured equivalent doses for each OSL sample**

**Table 7  
Equivalent Dose, Mean and Minimum Age Model**

<b>1094.010</b>						
<b>Sample</b>	<b># of Aliquots</b>	<b>Mean De (Gy)</b>	<b>Error</b>	<b>MAM De (Gy)</b>	<b>Error</b>	
TUOSL 22	36	2.29	0.58	2.11	0.04	
TUOSL 23	57	2.36	0.42	2.2	0.07	

**1094.059**

<b>Sample</b>	<b># of Aliquots</b>	<b>Mean De (Gy)</b>	<b>Error</b>	<b>MAM De (Gy)</b>	<b>Error</b>
TUOSL 26	46	2.09	0.62	1.83	0.08
TUOSL 27	17	1.43	0.95	-	-
TUOSL 28	39	3.07	0.78	2.78	0.02
TUOSL 29	10	2.71	0.2	-	-

**1094.084**

<b>Sample</b>	<b># of Aliquots</b>	<b>Mean De (Gy)</b>	<b>Error</b>	<b>MAM De (Gy)</b>	<b>Error</b>
TUOSL 30	35	3.38	1.12	2.59	0.1
TUOSL 31	39	3.11	0.75	2.57	0.04
TUOSL 32	21	2.55	0.13	-	-

**1094.046**

<b>Sample</b>	<b># of Aliquots</b>	<b>Mean De (Gy)</b>	<b>Error</b>	<b>MAM De (Gy)</b>	<b>Error</b>
TU33	8	1.96	0.07	-	-
TU35	9	3.42	0.26	-	-

Ages ranged from  $0.46 \pm 0.03$  ka to  $1.13 \pm 0.10$  ka for fine-grained samples and  $0.71 \pm 0.05$  ka to  $1.20 \pm 0.07$  ka for coarse-grained samples. The ages are plotted on the lithology plots in Fig. 9. Fine-grained samples consistently gave an underestimation of the age, perhaps due to undetected feldspar contamination. Core 1094.010 and 1094.084 produce the most reliable accretion rate calculations because the ages of the crevasse splay were estimated with coarse-grains. With underestimated ages for TUOSL 27 and 29, it is not possible to produce reliable accretion rates for the crevasse splay deposits at core 1094.059. Core 1094.046 dates multiple

depositional events, so its accretion rate is represented as an average rate over a period >300 years.

A natural crevasse typically has a life span of 25 to 175 years, depending on factors of size, water and sediment discharge, and wind and tidal influences (Wells and Coleman, 1987). Knowing the depths and ages of samples, it is possible to obtain accretion rates of the Attakapas Splay, using a simple rate equation of difference between depths within a core divided by the difference between ages. Table 9 shows that accretion rates range from ~0.7 to 2.5 cm yr<sup>-1</sup>. Core 1094.010's accretion rate was measured using the most conservative age difference, dividing 300 cm of depths by 120 years. This provides the most conservative vertical accretion rate at that core. It was not possible to date individual depositional events of cores 1094.059 and .084 with the data, but the averaged accretion rate can provide insight on the long-term viability of crevasse splays. Qualitative and quantitative observations of these cores also show that depositional events from crevasse splays can create ~3-9 m of vertical land, which would be needed to restore coastal wetlands in Louisiana. With these accretion rates, comparisons can be made between accretion rates from a crevasse splay to current relative sea-level rise and the viability of crevasse splay river diversions can be discussed.

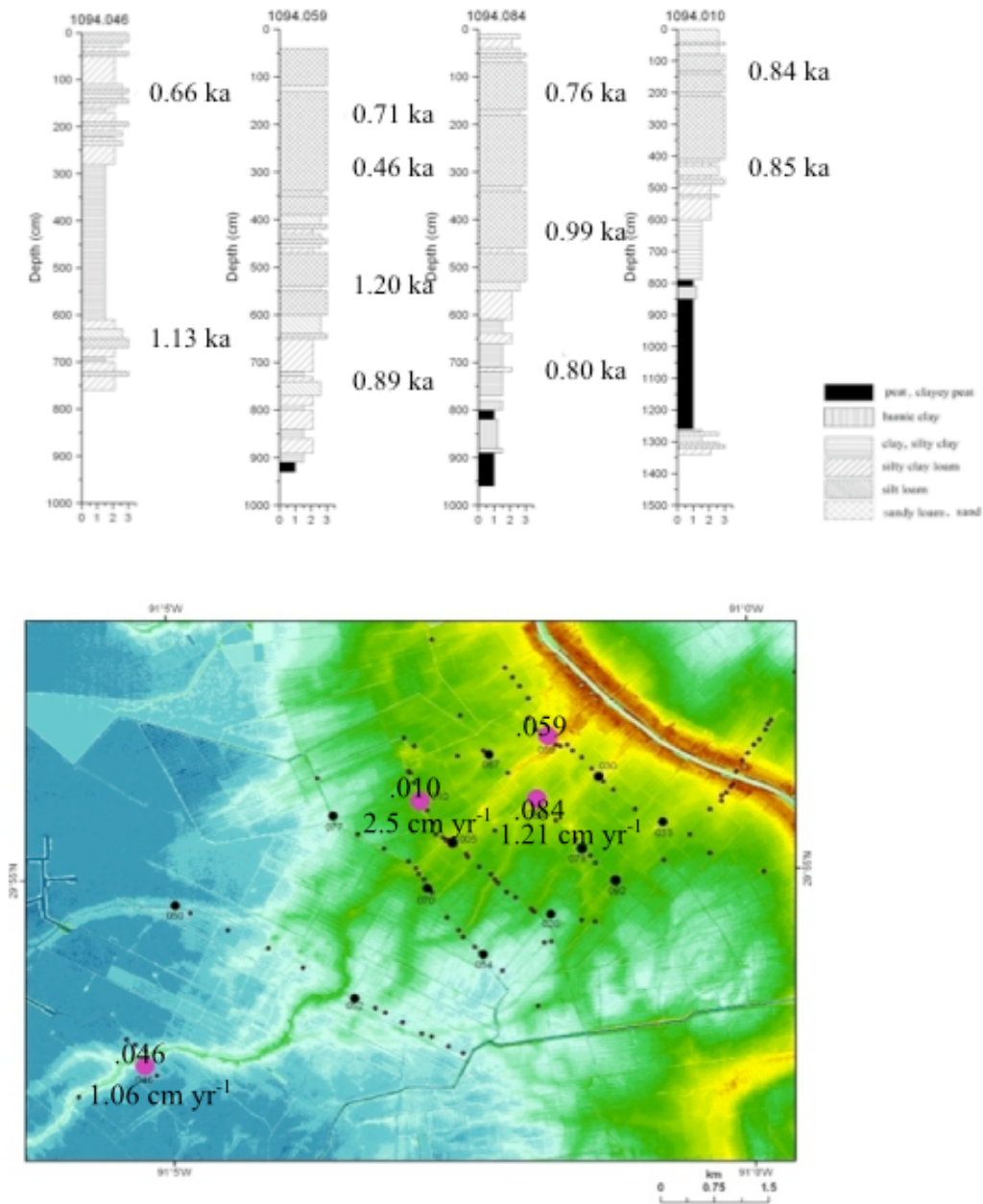


**Figure 9. LIDAR map with cores and lithology plots of cores dated with OSL.** Cores 1094.046, .010, .059, & .084 were dated with OSL. The accretion rates measured as 1.06, 2.5, and 1.21 cm yr<sup>-1</sup>, respectively. Highest vertical accumulation rates occurred nearest the channel. Core .010 dates a single event and created 3 m of vertical land in ~120 years. Core .084 shows that two depositional events occurring for 250 years created 2.8 m of land at an averaged rate of 1.21 cm yr<sup>-1</sup>. Core .046, furthest from the channel, shows an accretion rate of 1.06 cm yr<sup>-1</sup>. Core .059 created 9 vertical meters of land.

**Table 8**  
**Age Estimates**

**1094.010**

<b>Sample</b>	<b>Depth (cm)</b>	<b>Texture</b>	<b>Age (ka)</b>	<b>Error</b>
TUOSL 22	110-120	SL	0.84	0.05
TUOSL 23	410-420	SiL	0.85	0.06

**1094.059**

<b>Sample</b>	<b>Depth (cm)</b>	<b>Texture</b>	<b>Age (ka)</b>	<b>Error</b>
TUOSL 26	190-200	vfs-fs	0.71	0.05
TUOSL 27	300-310	SL	0.46	0.03
TUOSL 28	530-540	SL	1.20	0.07
TUOSL 29	720-730	SiCL	0.89	0.09

**1094.084**

<b>Sample</b>	<b>Depth (cm)</b>	<b>Texture</b>	<b>Age (ka)</b>	<b>Error</b>
TUOSL 30	130-140	SL	0.76	0.07
TUOSL 31	410-420	vfs	0.99	0.06
TUOSL 32	690-700	SiC	0.80	0.05

**1094.46**

<b>Sample</b>	<b>Depth (cm)</b>	<b>Texture</b>	<b>Age (ka)</b>	<b>Error</b>
TU33	140-150	SiL	0.66	0.10
TU35	650-660	SiL	1.13	0.10

**Table 9**  
**Accretion rates for each core**

Core	Vertical Accretion (cm)	Time (years)	Accretion rate (cm yr <sup>-1</sup> )
1094.010	300	10-120	2.5 ( <i>minimum</i> )
1094.059	340	470	0.69 ( <i>coarse</i> )
	420	590	0.98 ( <i>fine</i> )
1094.084	280	250	1.21
1094.046	510	420	1.06

## 6. Discussion

The three essential issues that need to be addressed when designing major river diversions are the amount of sediment being delivered, the amount of land created by the diversion, and the stability of continued growth (Winer & Raphael, 2005). This paper examines issues of vertical land creation and the stability of continued growth and looks to quantify wetland accretion rates of a recent crevasse splay to use as an analog for Mississippi River diversions. Our preliminary findings show that continued crevassing at the Attakapas Splay had accretion rates ranging from ~0.7 to 2.5 cm yr<sup>-1</sup>. This event deposited mostly silty and sandy sediment. A Holocene peat layer beneath the Attakapas Splay indicates that this area was originally a swamp-like environment. Thus, this study provides insight onto the possibility of a river diversion into a swampy environment.

Global eustatic sea-level rise is predicted to rise at ~0.3 cm yr<sup>-1</sup> (IPCC, 2007). Estimates in southern Louisiana suggest that sea-level rise is occurring at a rate as high as ~1 cm yr<sup>-1</sup> due to

the adding compaction of Holocene deposits (Gonzalez and Törnqvist, 2006). Estimates of the Attakapas Splay represent an event before human alteration of the Mississippi River (dams, levees, decrease in sediment supply) and may suggest a “best case scenario” of a naturally crevassing river diversion. Estimates of an accretion rate of  $\sim 0.7$  to  $2.5 \text{ cm yr}^{-1}$  suggest that a river diversion would aid coastal restoration. Core 1094.059, which is within the major feeder channel, created  $\sim 9$  m of vertical land in  $\sim 600$  years. Core 1094.010, a core further away from the major feeder channel that dated a single depositional event, shows the best insight for a single crevassing event and the short-term implications of a river diversion. The vertical accretion rate of  $\sim 2.5 \text{ cm yr}^{-1}$  is higher than RSL rise in the greater subsiding areas ( $\sim 1 \text{ cm yr}^{-1}$ ) and thus shows that crevasse splay diversions have significant potential in restoring wetlands in the short-term (100 years). The accretion rate of the single splay event 1094.010 is higher than current estimates of accretion rates in artificially managed crevasses at the Caernavron study site ( $\sim 1.5 \text{ cm yr}^{-1}$ ) (Lane et al., 2006).

While vertical accretion rates in this study suggest that a river diversion should be capable of maintaining and rebuilding Louisiana wetlands, the effectiveness of a diversion depends on the underlying Holocene strata that dictate compaction rates. Compaction rates range from  $\sim 0.5$ - $1 \text{ cm yr}^{-1}$  and can lead up to a loss of  $\sim 1/3^{\text{rd}}$  of surface elevation gain (Törnqvist, 2008). This suggests that high sediment fluxes are required to offset shallow compaction. With this estimate of compaction, the net vertical elevation rate would be  $>1.5 \text{ cm yr}^{-1}$ , meaning that there is still sufficient sediment flux to overcome relative sea-level rise. Successful coastal restoration will be achieved by not just estimating vertical accretion rates, but net surface elevation gain and the underlying sediment architecture.

The implications of this study suggest that a river diversion would serve as a means to mitigate or even reverse coastal wetland loss, and potentially increase landmass. This study shows that vertical accretion can be  $\sim 2.5 \text{ cm yr}^{-1}$  for single crevassing events, while long-term scale vertical growth can be upwards of 9 meters in 600 years, with rates as high as  $1.21 \text{ cm yr}^{-1}$ . The actual impact of a river diversion will differ based on the location of the diversion. Decreased sediment loads must be taken into account with current restoration plans. With a decreased sediment supply, it is likely that the accretion rates would be less in the present. Therefore, coastal restoration plans should focus on areas of high importance, such as socioeconomically critical areas of Louisiana. Restoration efforts should account for the potential for high accretion rates and stability, the engineering feasibility, costs and benefits, and the socioeconomic impact. This study shows that if the Attakapas Splay is used as an analog for river diversions, accretion rates can be enough to sustain wetlands, while also creating new land, and that crevassing events are viable long-term, on a 100-year scale.

## 7. Conclusions

Optically stimulated luminescence is seen as a reliable estimator of depositional ages of Quaternary sediment. This study aimed to determine accretion rates of the Attakapas Splay at four sites using OSL. Coarse-grained sediment consistently produced more reliable equivalent dose estimates than fine-grained, probably due to feldspar contamination. Estimates suggest accretion rates to be between  $\sim 0.7 \text{ cm yr}^{-1}$ , long-term, and  $2.5 \text{ cm yr}^{-1}$  for single depositional events. These estimates are in line with or greater than current rates of managed splay diversions in the MRD. Compared to RSL, a river diversion using a crevassing event can serve as a way to adapt and prevent continued land loss. The Bayou Lafourche study area suggests a sediment and

water supply analogous to the present day Mississippi River and could be a good model for diversions of the river. The preliminary findings show that there is potential for significant environmental and economic benefit in creating river diversions through crevassing, even after factoring in Holocene compaction. Core 1094.010 shows rapid deposition of 3 m in <120 years. More work is needed for a better resolution of accretion rates in cores 1094.049, .084, and .046 because they date multiple depositional events; however, the potential for significant and sustained vertical land growth shown at this site, suggests that policy should include crevasse splay diversions in any Louisiana coastal restoration plans.

## 8. Acknowledgements

I would like to thank the Louisiana Sea Grant Program and their Undergraduate Research Opportunities Program for their generous grant to fund this research, as well as coworkers, Jon Marshack, and Jennifer Kuykendall, advisor and coworker Zhixiong Shen for his help in the field, lab, and editing, and advisor Torbjörn Törnqvist. I would also like to thank the Geography Department of the University of Liverpool, for allowing for the use of their facilities for this project.

## 9. References

- Adamic G. & Aitken, M.J., (1998). Dose-rate conversion factors: update. *Ancient TL* 16 (2): 37-50.
- Aitkin, M.J. (1998). *An Introduction to Optical Dating: The Dating of Quaternary Sediments by the Use of Photon-stimulated Luminescence*. New York, N.Y: Oxford University Press.

- Allison, M.A. & Meselhe, E.A. (2010). The use of large water and sediment diversions in the lower Mississippi River (Louisiana) for coastal restoration. *Journal of Hydrology*, 287, 346-360.
- Arnold, L.J. et al. (2007). Statistical treatment of fluvial dose distributions from Colorado arroyo deposits. *Quaternary Geochronology* 2: 162–167
- Aslan, A. & Autin, W.J. (1999). Evolution of the Holocene Mississippi River Floodplain, Ferriday, Louisiana: Insights on the Origin of Fine-grained Floodplains. *Journal of Sedimentary Research*, 69 (4): 800-815.
- Bailey, R.M., et al. (1997). Partial bleaching and the decay from characteristics of quartz OSL. *Radiation Measurements*, 27 (2): 123-136.
- Blum, M. D. et al (2008). Ups and downs of the Mississippi delta. *Geology* 36, 675-678.
- Blum, M.D. & Roberts, H.H. (2009). Drowning of the Mississippi Delta due to insufficient sediment supply and global sea-level rise. *Nature Geoscience*. 2, 288-491.
- Coleman, J.M., et al (1998) Mississippi River Delta: An Overview. *Journal of Coastal Research* 14 (3): 698-716.
- Day, J.W. et al. (2007). Restoration of the Mississippi Delta: Lessons from Hurricanes Katrina and Rita. *Science*, 315: 1679-1684
- Duller, G.A.T. (2008). Single grain optical dating of Quaternary sediments: why aliquot size matters in luminescence dating. *Boreas* 37: 589-612.
- Galbraith, R.F. et al. (1999). Optical dating of single and multiple grains of quartz from Jinnium rock shelter, northern Australia: Part I. *Archaeometry* 41, 339–364.

- Gagliano, S.M. et al. (1981). Land Loss in Mississippi River Deltaic Plain. *AAPG Bulletin-American Association of Petroleum Geologists*, 65 (9)
- Gonzales, J. L. & Törnqvist, T. E. (2006). Coastal Louisiana in crisis: Subsidence or sea level rise? *Eos* 87, 493-498
- IPCC, 2007: Summary for Policymakers. In: *Climate Change 2007: The Physical Science Basis. Contribution of Working Group I to the Fourth Assessment Report of the Intergovernmental Panel on Climate Change* [Solomon, S., D. Qin, M. Manning, Z. Chen, M. Marquis, K.B. Averyt, M. Tignor and H.L. Miller (eds.)]. Cambridge University Press, Cambridge, United Kingdom and New York, NY, USA
- Lane, R.R. et al. (2006). Wetland surface elevation, vertical accretion, and subsidence at three Louisiana estuaries receiving Mississippi River water. *Wetlands*, 26 (4): 1130-1142.
- Louisiana Coastal Wetlands Conservation and Restoration Task Force and the Wetlands Conservation and Restoration Authority. (1998). *Coast 2050: Toward a Sustainable Coastal Louisiana*. Louisiana Department of Natural Resources. Baton Rouge, La.
- Mauz, B. et al. (2006). The alpha efficiency of silt-sized quartz: New data obtained by single and multiple aliquot protocols. *Ancient TL* 24, 47-52.
- Mauz, B. and Lang, A. (2004a). Removal of the feldspar-derived luminescence component from polymineral fine silt samples for optical dating applications: evaluation of chemical treatment protocols and quality control procedures. *Ancient TL* 22, 1-8.
- Mauz, B. and Lang, A. (2004b). The dose rate of beta sources for optical dating applications: A comparison between fine silt and fine sand quartz. *Ancient TL* 22, 45-48
- Murray, A.S., Roberts, R.G., 1998. Measurement of the equivalent dose in quartz using a regenerative-dose single-aliquot protocol. *Radiation Measurements* 29, 503-515.

- Murray, A.S., Wintle, A.G., 2000. Luminescence dating of quartz using an improved single-aliquot regenerative-dose procedure. *Radiation Measurements* 32: 57–73.
- Murray, A.S. & Wintle, A.G. (2003). The single aliquot regenerative dose protocol: Potential for improvements in reliability. *Radiation Measurements* 37, 377-381.
- Olley, J.M. (2004). Optical dating of Holocene sediments from a variety of geomorphic settings using single grains of quartz. *Geomorphology* 60: 337-358.
- Paola, C. et al. (2010). Natural Processes in Delta Restoration: Application to the Mississippi Delta. *Annual Review of Marine Science* 3: 3.1-3.25
- Richardson, J.A & Scott, L.C. (2004). The Economic Impact of Coastal Erosion in Louisiana on State, Regional, and National Economics, Louisiana Department of Natural Resources. Baton Rouge, La
- Thomsen, K.J. (2004). Optically stimulated luminescence: Techniques in retrospective dosimetry using single grains of quartz extracted from Unheated Materials. Risø PhD thesis. Risø National Laboratory, Denmark.
- Törnqvist, T. E. et al. (1996). A revised chronology for Mississippi River subdeltas. *Science* 273, 1693-1696
- Törnqvist, T. E. et al. (2006). How stable is the Mississippi Delta? *Geology*, 34: 697-700
- Törnqvist, T. E. et al. (2008). Mississippi Delta subsidence primarily caused by compaction of Holocene strata. *Nature Geoscience*. 1, 173-176.

- Troutman, J. & MacInnes, A.D. (1999). Coast 2050 Region 2: Channel Armor Gap  
Crevasse MR-06 (XMR-10). Louisiana Department of Natural Resources. Baton Rouge,  
La.
- Wells, J.T. & Coleman, J.M. (1987). Wetland loss and the subdelta life cycle. *Estuarine, Coastal  
and Shelf Science*, 25: 111-125.
- Winer, H.S. & Raphael, N.K., (2005) Mississippi River Sediment Diversions. Proceedings of the  
14<sup>th</sup> Biennial Coastal Zone Conference. Baton Rouge, La.
- Wintle, A.G. & Murray, A.S. (2006). A review of quartz optically stimulated luminescence  
characteristics and their relevance in single-aliquot regeneration dating protocols.  
*Radiation Measurements* 41, 369-391.